Journal of Computational and Applied Mathematics 319 (2017) 141–158

Contents lists available at ScienceDirect

Journal of Computational and Applied Mathematics

journal homepage: www.elsevier.com/locate/cam

An isogeometric boundary element method using adaptive integral method for 3D potential problems

Y.P. Gong, C.Y. Dong*

Department of Mechanics, School of Aerospace Engineering, Beijing Institute of Technology, Beijing 100081, China

HIGHLIGHTS

- A general method is proposed to calculate the nearly singular integrals appearing in the 3D IGABEM.
- The boundary element integrations can be computed easily and effectively at optimal computational cost.
- The adaptive algorithm can be used to cope with the common situation where the sizes of adjacent cells are significantly different.
- The power series expansion method is expanded to compute the singular integrals appearing in 3D IGABEM.

ARTICLE INFO

Article history:
Received 19 October 2016
Received in revised form 30 December 2016

Keywords:
Potential problem
3D IGABEM
Adaptive integration method
Power series expansion method

ABSTRACT

Due to the merits of exact geometrical representation, high accuracy, no meshing process, and only the boundary description of the problem etc., the isogeometric boundary element method, i.e. IGABEM, has achieved rapid development. In this paper, based on the upper bound of the relative error of the Gaussian quadrature formula, we presented a 3D IGABEM using adaptive integration method for potential problems. This method offers a number of key improvements compared with conventional IGABEM. Firstly, the boundary element integrations can be computed easily and effectively at optimal computational cost. Secondly, the adaptive algorithm can cope with the common situation where the sizes of adjacent cells are significantly different. Moreover, the presented method can compute the nearly singular integrals easily, owing to the use of subdivision technique. To accurately evaluate the singular integrals appearing in our method, the power series expansion method is employed. The integration surface is on the real surface of the model, rather than the interpolation surface, i.e. no geometrical errors. Thus, the value of integral is more accurate than the traditional boundary element method, which can improve the computation accuracy of the IGABEM. Numerical tests show that the presented method has good performance in both exactness and convergence.

1. Introduction

Since the framework of isogeometric analysis (IGA) method was established by Hughes et al. [1], the IGA method has been widely used in fluid problems [2–4], structural vibrations [5], structural eigenvalue problems [6], shape optimization [7], gradient elasticity [8], contact problems [9], shell analysis [10,11] and so on. Due to the merits of high accuracy and only the boundary description of the problem, the isogeometric boundary element method, i.e. IGABEM, has achieved rapid development recently [12–14] and has successfully been applied to investigate various problems, e.g. elasticity problems

* Corresponding author.
E-mail address: cydong@bit.edu.cn (C.Y. Dong).

http://dx.doi.org/10.1016/j.cam.2016.12.038
0377-0427/

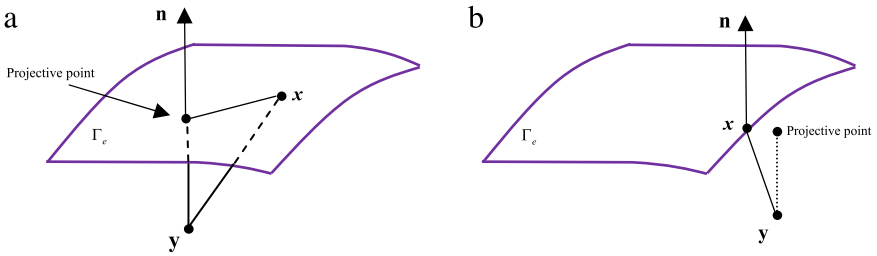

Fig. 1. Definition of the projective point from the source point **y** to the 3D surface element.

[15,16], potential problems [17], Laplace equation [18], fast multipole IGABEM [19,20], Helmholtz problems [21], ship wave-resistance problem [22,23], acoustic problems [24,25], shape optimization [26–28], nonsingular IGABEM analysis [29], weakly-singular integral equation [30], crack problem [31] and adaptive mesh-refinement [32].

Different from conventional BEM, the basis function of IGABEM is chosen to exactly capture the geometry. This function is also used to approximate the unknown fields. When the procedure of refinement is acquired for the unknown fields, the exact geometry will be maintained at all stages of analysis. This is a distinct advantage over traditional BEM, in which the geometrical errors will greatly influence the accurate of the numerical result, especially for complex models or thin-body/coating structures. For IGABEM, it is obvious that only very little boundary elements are needed to exactly describe the boundary geometry. Therefore, the area of one isogeometric element will be much larger than that of traditional BEM. As we have known, it is vitally important to compute the integration accurately and efficiently over the surface of isogeometric element. Obviously, the problem can be solved by increasing the Gauss integration order. However, the kernel functions will be evaluated many millions of times and the computational cost will be increased rapidly.

Gao and Davies [33,34] presented an adaptive integration method based on the upper bound of the relative error of the Gaussian quadrature formula for traditional BEM by eliminating the unnecessary function evaluations. In this method, a specified maximum of Gauss order is given beforehand. In the computation, if the required Gauss integration order exceeds the maximum, the integration elements will be divided into sub-elements. The boundary element integration can be computed easily and effectively at optimal computational cost. Further, the adaptive algorithm can cope with the common situation where the sizes of adjacent cells are significantly different. So the adaptive integration method can solve the computation of the integration on larger isogeometric elements perfectly. Here, we extend the method to 3D IGABEM, which delivers high accuracy at minimum computational cost for 3D boundary integrals on isogeometric element.

It is possible to compute the physical quantities of points very close to the real boundary with small number of boundary elements, due to the characteristics of exact geometrical representation of IGABEM. However, when the computed points are very close to the real boundary of the model, the nearly singular integrals appear, which covers up the advantage of the IGABEM. The adaptive integration method is based on element sub-division technique, so the nearly singular integrals appearing in the IGABEM can be computed effectively. In addition, although various methods have been proposed to deal with the nearly singular integrals appearing in conventional BEM [35–38], many of the methods deal with the case when the projective point of the evaluation point is located in the element (see Fig. 1(a)). For these methods, the line consisting of the evaluation point and the projection point must be perpendicular to the tangential plane through the projection point. However, the methods fail when the projective point of the evaluation point is located outside the element (see Fig. 1(b)) which will be often encountered in some complex computational models [39]. For this case, the adaptive integration method can easily and precisely compute the integrals in Fig. 1(b).

As we have known, in the implementation of conventional BEM, varied orders of singular integrals appear and so is IGABEM. All the singular integrals appearing in 3D IGABEM require careful study and analysis. Over the past two decades, some considerable efforts were devoted to proposing novel computational algorithms that circumvent or greatly eliminate the singularity issues associated with the boundary element analysis. They usually include but are not limited to, analytical and semi-analytical one [40,41], new Gaussian quadrature [42], the local regularization method [43,44], transformation method [45–47], finite-part integral [48,49], subtraction technique [50,51], etc. Among these methods, the local regularization technique proposed by Guiggiani et al. [52,53] was extensively employed to remove various orders of singularities. Although the method was successfully used to evaluate the strong singular integral appearing in 2D IGABEM [14,15], it requires the expansion of all quantities of the integrand into Taylor's series, which may be arduous and computationally expensive [54]. The power series expansion method [55,56], presented by Gao, seems to be a more accurate and flexible method for evaluating 2D or 3D singular boundary integrals by expressing the non-singular part of a singular integrand as well as the global distance r as power series in the local distance ρ of the intrinsic coordinate system.

In this paper, the singular integrals appearing in the 3D IGABEM will be computed by the power series expansion method. Firstly, the singular surface integral is divided into a line integral over the contour of the integration surface and a radial integral containing the singularities by the radial integration method (RIM) [57,58]. Then the singularities condensed in the radial integral are removed analytically or numerically by extracting the finite value parts from the power series expansions. Finally, the line integral with regular kernel functions can be computed by the standard Gaussian quadrature. Through the

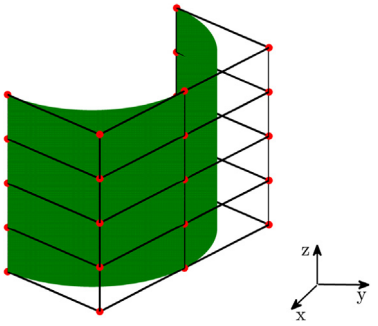

Fig. 2. A bi-quadratic NURBS surface. Knot vectors are $\mathbf{U} = \mathbf{V} = \{0, 0, 0, 0.5, 0.5, 1, 1, 1\}$. The 5×5 control points are denoted by red filled circles. (For interpretation of the references to color in this figure legend, the reader is referred to the web version of this article.)

above procedure, singular integrals over isogeometric boundary elements can be evaluated with high accuracy, even when the order of singularity is high.

A brief outline of this paper is as follows. Section 2 introduces necessary background concepts. Section 3 presents the adaptive integration method for 3D boundary integrals on isogeometric element. Section 4 gives the detailed computational procedure of power series expansion method for singular integrals appearing in 3D IGABEM. Several numerical examples are given in Section 5 to verify the efficiency and accuracy of the present method. Finally, we present the conclusions for our work.

2. Methodology

2.1. NURBS basis functions and NURBS surfaces

In the present work, NURBS basis functions which are the most common in CAD software are used. A NURBS surface is fully defined by the following items [1,14,15]:

- Two knot vectors for each parametric direction $\mathbf{U}\{= \xi_1, \xi_2, \ldots, \xi_{n+p+1}\}$ and $\mathbf{V}\{= \eta_1, \eta_2, \ldots, \eta_{m+q+1}\}$. Note that n and m are respectively the numbers of basis functions along parametric directions ξ and η, whereas p and q are the corresponding polynomial orders.
- A control net of points $\{P_{i,j}\}$, $1 \leq i \leq n$, $1 \leq j \leq m$.

Mathematically, a tensor-product NURBS surface can be represented as follows:

$$S(\xi, \eta) = \sum_{i=1}^{n} \sum_{j=1}^{m} R_{i,j}^{p,q}(\xi, \eta) P_{i,j} \tag{1}$$

where $S(\xi, \eta)$ is the vector with Cartesian coordinates of the point described by the parametric point $\xi_1 \leq \xi \leq \xi_{n+p+1}$ and $\eta_1 \leq \eta \leq \eta_{m+q+1}$. The bivariate basis functions $R_{i,j}^{p,q}$ are given by

$$R_{i,j}^{p,q}(\xi, \eta) = \frac{N_{i,p}(\xi) M_{j,q}(\eta) \omega_{i,j}}{\sum_{\hat{i}=1}^{n} \sum_{\hat{j}=1}^{m} N_{\hat{i},p}(\xi) M_{\hat{j},q}(\eta) \omega_{\hat{i},\hat{j}}} \tag{2}$$

where $N_{i,p}$ is the ith B-spline basis function of order p and $M_{j,q}$ is the jth B-spline basis function of order q. $\omega_{i,j}$ is the positive weight corresponding to the control point $P_{i,j}$. The B-spline basis functions of degree 0 are defined as

$$N_{i,0} = \begin{cases} 1 & \text{if } \xi_i \leq \xi < \xi_{i+1}, \\ 0 & \text{otherwise} \end{cases} \tag{3}$$

where $1 \leq i \leq n$, n is the number of basis functions which form the B-spline.

For higher degrees,

$$N_{i,p}(\xi) = \frac{\xi - \xi_i}{\xi_{i+p} - \xi_i} N_{i,p-1}(\xi) + \frac{\xi_{i+p+1} - \xi}{\xi_{i+p+1} - \xi_{i+1}} N_{i+1,p-1}(\xi). \tag{4}$$

An example of a NURBS surface is shown in Fig. 2. Fig. 3 gives the basis functions of the NURBS surface and the corresponding parameter space.

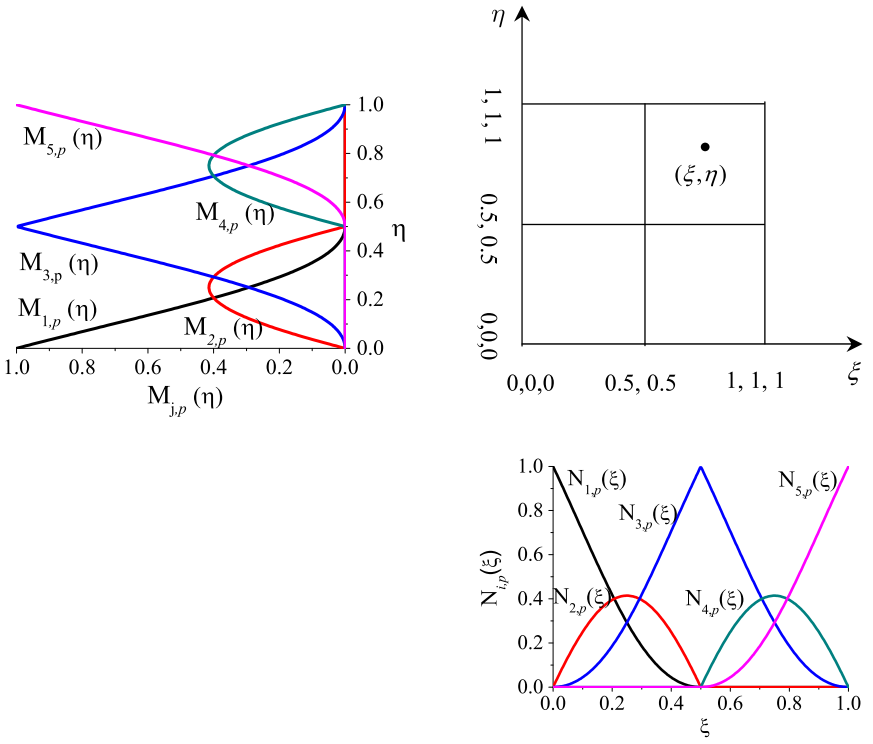

Fig. 3. The basis functions of the NURBS surface and the corresponding parameter space.

2.2. The IGABEM for potential problems

Considering the boundary integral equation of 3D potential problems in the domain Ω enclosed by boundary Γ. The usual direct BEM formulation is presented as follows [17,39]:

$$c(\mathbf{y})u(\mathbf{y}) = \int_{\Gamma} q(\mathbf{x})u^*(\mathbf{x},\mathbf{y})d\Gamma(\mathbf{x}) - \int_{\Gamma} u(\mathbf{x})q^*(\mathbf{x},\mathbf{y})d\Gamma(\mathbf{x}) \tag{5}$$

where $\mathbf{y}$ and $\mathbf{x}$ are the source and the field points, respectively. $c(\mathbf{y})$, usually being $c(\mathbf{y}) = 1/2$ for a smooth boundary, is a coefficient which depends only on the local geometry of Γ at point y. $u^*(\mathbf{x},\mathbf{y})$ represents the fundamental solution for 3D potential problems expressed as

$$u^*(\mathbf{x},\mathbf{y}) = \frac{1}{4\pi r} \tag{6}$$

and $q^*(\mathbf{x},\mathbf{y})$ is its normal derivative

$$q^*(\mathbf{x},\mathbf{y}) = \frac{\partial u^*(\mathbf{x},\mathbf{y})}{\partial r}\frac{\partial r}{\partial \mathbf{n}} \tag{7}$$

where r denotes the distance between the source and the field points. $\mathbf{n}$ is the unit outward normal direction to the boundary Γ, with components n_i, $i = 1, 2, 3$.

For the purpose of numerical computation, the boundary surface Γ should be discretized into a non-overlapping set of N_e elements, i.e.

$$\Gamma = \bigcup_{e=1}^{N_e} \Gamma_e, \qquad \Gamma_i \cap \Gamma_j = 0, \quad i \neq j.$$

In the implementation of 3D IGABEM, we use two knot vectors $\mathbf{U}$ and $\mathbf{V}$, $m \times n$ control points $\{P_{i,j}\}$, $i = 1, 2, \ldots, n, j = 1, 2, \ldots, m$ and curve orders p and q to build the boundary shape and the basis functions. The integral elements are defined in the parametric space as non-zero knots span $[\xi_i, \xi_{i+1}] \times [\eta_j, \eta_{j+1}]$, where $\xi_i, \ \xi_{i+1} \in \mathbf{U}$ and $\eta_j, \ \eta_{j+1} \in \mathbf{V}$. In order to carry out the numerical integration using Gauss–Legendre quadrature, local coordinate $\bar{\xi}$ and $\bar{\eta}$ must be in the range $[-1, 1] \times [-1, 1]$. Therefore, there should be a transformation from the parameter space $(\xi, \eta) \in [\xi_i, \ \xi_{i+1}] \times [\eta_j, \ \eta_{j+1}]$ (ξ_i is the ith knot in $\mathbf{U}$ and η_j is the jth knot in $\mathbf{V}$, i and j are respectively the knot indexes in directions ξ and η) to the Gauss–Legendre range $[-1, 1] \times [-1, 1]$.

The Jacobian of transformation from the physical domain to a parametric domain is given by

$$\left|J_{(\xi\eta)}\right| = \left[\left(\frac{\partial x_2}{\partial \xi}\frac{\partial x_3}{\partial \eta} - \frac{\partial x_3}{\partial \xi}\frac{\partial x_2}{\partial \eta}\right)^2 + \left(\frac{\partial x_3}{\partial \xi}\frac{\partial x_1}{\partial \eta} - \frac{\partial x_1}{\partial \xi}\frac{\partial x_3}{\partial \eta}\right)^2 + \left(\frac{\partial x_1}{\partial \xi}\frac{\partial x_2}{\partial \eta} - \frac{\partial x_2}{\partial \xi}\frac{\partial x_1}{\partial \eta}\right)^2\right]^{1/2} \tag{8}$$

and Jacobian of the transformation from the parent domain to a parametric domain reads

$$\left|J_{(\bar{\xi}\bar{\eta})}\right| = \frac{1}{4}\left(\xi_{i+1} - \xi_i\right)\left(\eta_{j+1} - \eta_j\right). \tag{9}$$

To approximate the geometry and unknown fields, the non-zero basis functions must be determined for a particular element. After this is done, a set of local basis functions that are related to the global basis functions are given as

$$N_b^e(\bar{\xi}, \bar{\eta}) \equiv R_a^{p,q}(\xi(\bar{\xi}), \eta(\bar{\eta}))$$

where the local basis function number b, element number e and global basis function number are related by $a = \mathrm{conn}(e, b)$, where conn() is a connectivity function. Up to now, the geometry, potential and flux can be easily interpolated as

$$\begin{aligned} \mathbf{x}_e(\xi, \eta) &= \sum_{b=1}^{(p+1)(q+1)} N_b^e(\xi, \eta)\mathbf{x}_b \\ u_e(\xi, \eta) &= \sum_{b=1}^{(p+1)(q+1)} N_b^e(\xi, \eta)d_b \\ q_e(\xi, \eta) &= \sum_{b=1}^{(p+1)(q+1)} N_b^e(\xi, \eta)t_b \end{aligned} \tag{10}$$

where $\mathbf{x}_b$, d_b and t_b represent the coordinate, potential and flux coefficients at a particular control point.

Thus, we can obtain the 3D isogeometric boundary integral equation as follows

$$\begin{aligned} &C(\mathbf{x}')\sum_{l=1}^{(p+1)(q+1)} N_l^{\bar{e}}(\bar{\xi}', \bar{\eta}')d^{l\bar{e}} + \sum_{e=1}^{N_e}\sum_{l=1}^{(p+1)(q+1)}\left[\int_{-1}^{1}\int_{-1}^{1} q^*\left(\mathbf{x}', \mathbf{x}\left(\bar{\xi}, \bar{\eta}\right)\right)N_l^e(\bar{\xi}, \bar{\eta})J(\bar{\xi}, \bar{\eta})d\bar{\xi}d\bar{\eta}\right]d^{le} \\ &= \sum_{e=1}^{N_e}\sum_{l=1}^{(p+1)(q+1)}\left[\int_{-1}^{1}\int_{-1}^{1} u^*\left(\mathbf{x}', \mathbf{x}\left(\bar{\xi}, \bar{\eta}\right)\right)N_l^e(\bar{\xi}, \bar{\eta})J(\bar{\xi}, \bar{\eta})d\bar{\xi}d\bar{\eta}\right]t^{le} \end{aligned} \tag{11}$$

where x' represents the collocation point and $\bar{\xi}'$ and $\bar{\eta}'$ represent the local coordinates of the collocation point on element $\bar{e}$.

An important step in the implementation of the IGABEM is the accurate evaluation of various integrals arising in boundary integral equations (11). These integrals become singular or nearly singular when the calculation point **y** collides with or is very close to the integral element. Hence, nearly singular integrals appear in the discretized form of Eq. (10) so that the numerical integrations by the standard Gaussian quadrature fail. In addition, for 3D IGABEM only very little boundary elements are needed to exactly describe the boundary geometry. As a result, the area of one isogeometric element will be much larger than that of traditional BEM. Hence, it is very important that the singular integral, nearly singular integral and regular integral with larger integral domain should be accurately and efficiently evaluated.

In this paper, we will use the adaptive integration method to deal with the regular and nearly singular boundary integrals on isogeometric element. Nearly singular integrals are not singular in the sense of mathematics. So the adaptive integration technique based on element sub-division can effectively eliminate nearly singular integrals appearing in the IGABEM. In the implementation of BEM, the accurate evaluation of the singular integrals is also a crucial and difficult task. Here both the strongly and weakly singular integrals in 3D IGABEM are computed by the power series expansion method [56]. The implementation is detailed in the following sections.

3. Adaptive integration scheme for 3D boundary integral on isogeometric element

For standard Gauss quadrature the integral of a function $f(x)$ between arbitrary limits (a, b) can be approximated by the weighted sum of a discrete number of function values, normally evaluated at certain sampling points (ordinates) between the two limits. In general, the Gaussian quadrature formula for a surface in three dimensions can be expressed in the intrinsic coordinate system by the equation

$$I = \int_{-1}^{1}\int_{-1}^{1} f(\xi, \eta)d\xi d\eta = \sum_{i=1}^{m_1}\sum_{j=1}^{m_2} w_1^i w_2^j f(\xi^i, \eta^j) + E_1 + E_2 \tag{12}$$

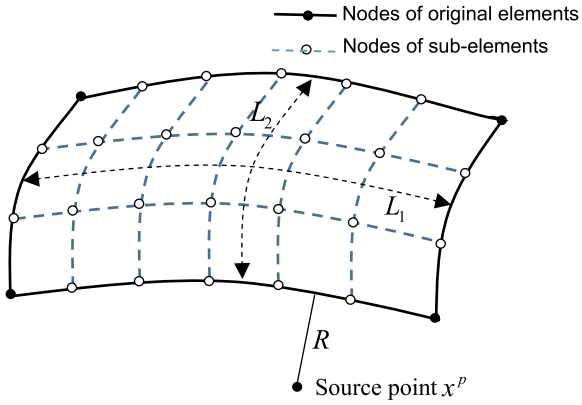

Fig. 4. Element sub-division technique.

where ξ^i, η^j are the Gauss ordinates, w_1^i, w_2^j are the weights, m_1, m_2 are the Gauss orders, and E_1, E_2 are the integration errors in the two directions. In 1984, Mustoe [59] proposed the following approximate formula for the upper bound of the relative error $e_i = E_i/I$ in the ith direction.

$$e_i \leq 2\left(\frac{L_i}{4R}\right)^{2m_i} \frac{(2m_i + p - 1)!}{(2m_i)!(p-1)!} \tag{13}$$

where p is the order of singularity of the integrand r^{-p}, L_i is the length of the element in the ith direction, and R is the minimum distance from the source point to the element, as shown in Fig. 4.

In order to avoid using excessively high Gauss orders m_i, the elements should be further divided into sub-elements to reduce the L_i/R ratio. It should be pointed out that, for this method, the nearly singular integrals can be accurately computed by using normal Gauss orders due to the ratio L_i/R will not be too large.

Based on the study of Davies and Bu [60], Eq. (13) can be approximated by the expression [33,34]

$$m_i = \sqrt{\frac{2}{3}q + \frac{2}{5}}\left[-0.1\ln\left(e_i/2\right)\right]\left[\left(8L_i/3R\right)^{3/4} + 1\right] \tag{14}$$

which can be rearranged to yield:

$$L_i = \frac{3}{8}R\left(\frac{-10m_i}{\sqrt{2q/3 + 2/5}\ln(e_i/2)} - 1\right)^{4/3}. \tag{15}$$

Using this approximation, the required Gauss order is obtained explicitly, rather than through iteration. Alternatively, given a maximal Gauss orders, the corresponding sub-element dimensions can be obtained explicitly. Now, in order to implement an adaptive integration scheme based on these criteria, it is necessary to devise efficient methods for determining the geometric parameters R and L for each collocation point and for each element, or sub-element. Details of derivation and implementation can be found in the literatures [33,34]. Here, we expand them to 3D IGABEM.

3.1. Calculation of sub-element length

In any isogeometric element, Cartesian coordinates can be determined from the control points, i.e.

$$\mathbf{x}_e(\xi, \eta) = \sum_{b=1}^{(p+1)(q+1)} N_b^e(\xi, \eta)\mathbf{x}_b \tag{16}$$

where $\mathbf{x}_b$ represents the coordinates at a particular control point.

In this paper, the length of a boundary element, in the ith intrinsic direction ($[\xi_l, \xi_{l+1}]$ or $[\eta_l, \eta_{l+1}]$) is defined by the length of the curve through the center of the element along the integration direction (as shown in Fig. 4). For three dimension case, the length of a boundary element can be accurately calculated using

$$L_i = \int_{\xi_l}^{\xi_{l+1}} \sqrt{\sum_{j=1}^{3}\left(\frac{\partial x_j}{\partial \xi_i}\right)^2} d\xi_i = \int_{-1}^{1} \sqrt{\sum_{j=1}^{3}\left(\sum_{b=1}^{(p+1)(q+1)} \frac{\partial N_b^e}{\partial \xi_i} x_b\right)^2} \frac{\xi_{l+1} - \xi_l}{2} d\xi_i. \tag{17}$$

3.2. Calculation of minimum distance R

To determine the minimum distance R from source point to an element, Gao and Davies [33,34] proposed a Newton–Raphson iterative scheme for traditional BEM. Here, the method is also used to the IGABEM.

Firstly, we begin with some starting guess (ξ_0) of the intrinsic coordinates of the source point and we let r_j^0 be the resulting error in the computation of the jth component of the global coordinates of the source point. Now, the notation r_j^k is used to denote the values after the kth iteration in the Newton–Raphson iterative scheme, that is:

$$r_j^k = \sum_{b=1}^{(p+1)(q+1)} N_b^e x_j^b - x_j \tag{18}$$

where x_j is the jth component of the global coordinates of the source point and x_j^b represents the jth component at a particular control point.

To obtain improved values of ξ_i, we expand this equation using Taylor's theorem:

$$r_j^{k+1} = r_j^k + \frac{\partial r_j}{\partial \xi_i}\Delta\xi_i = r_j^k + \sum_{b=1}^{(p+1)(q+1)} \frac{\partial N_b^e}{\partial \xi_i} x_j^b \Delta\xi_i \tag{19}$$

where $\Delta\xi_i$ are the changes in ξ_i. Setting $r_j^{k+1} = 0$, we can obtain using the Newton–Raphson iterative scheme:

$$\left[K^k\right]\{\Delta\xi\} = -\left\{r^k\right\} \tag{20}$$

where the coefficients of the matrix are:

$$\left[K_{ij}^K\right] = \sum_{b=1}^{(p+1)(q+1)} \frac{\partial N_b^e}{\partial \xi_i} x_j^b.$$

Unless the calculations are being carried out for a volume cell, there will be one less intrinsic coordinate than global coordinate. Hence Eq. (20) is over-prescribed. In that case, the least-squares approximation will suffice, i.e.

$$\left[K^k\right]^{\mathrm{T}}\left[K^k\right]\{\Delta\xi\} = -\left[K^k\right]^{\mathrm{T}}\left\{r^k\right\} \tag{21}$$

where the superscript T denotes the matrix transpose. Solving for $\{\Delta\xi\}$, the current values of ξ_i can be updated, thus

$$\xi_i^{k+1} = \xi_i^k + \Delta\xi_i. \tag{22}$$

We now make the assumption that the proximal point has the intrinsic coordinates defined by the following equations:

$$\begin{aligned} &\xi_i = \xi_i^{k+1}, && \left(\text{if } \xi_i \le \left|\xi_i^{k+1}\right| \le \xi_{i+1}\right) \\ &\xi_i = \xi_i, && \left(\text{if } \left|\xi_i^{k+1}\right| \le \xi_i\right) \\ &\xi_i = \xi_{i+1}, && \left(\text{if } \left|\xi_i^{k+1}\right| \ge \xi_{i+1}\right) \end{aligned} \quad . \tag{23}$$

The minimum distance can then be calculated from the Pythagoras theorem, that is:

$$R = \sqrt{\sum_{j=1}^{3} R_j^2}$$

where R_j is the jth Cartesian component of the minimum distance and is determined from the intrinsic coordinates of the proximal point.

3.3. Adaptive integration scheme

The adaptive integration scheme employs the element sub-division technique described above. In papers [33,34], the authors have used the scheme to conventional boundary element method. Here, we will expand the method to 3D IGABEM.

(1) Compute the elements of the integral boundary which are defined in the parametric space as non-zero knots span $[\xi_i,\ \xi_{i+1}] \times [\eta_j, \eta_{j+1}]$.
(2) Calculate element length L_i and minimum distance R from the source point in integral equation to elements.
(3) Calculate the Gauss order m_i with specified precision.
(4) If $m_i \le m_{\max}$, using Gaussian quadrature evaluates the integral.
(5) if $m_i > m_{\max}$, using $m_i = m_{\max}$ calculates the permitted maximum length $L_i^{\max}$.
(6) Divide element into equal sub-elements. And calculate the length of each sub-element L_i^s.
(7) Calculate the minimum distance R_n from the source point to the nth sub-element.
(8) Calculate the Gauss order m_i^n for the nth sub-element.
(9) Apply Gauss quadrature formulas to evaluate the integral over the sub-element.
(10) Repeat (7)–(9) for all sub-elements.

3.4. Nearly singular integral in general IGABEM formulation

The nearly singular integrals arising in 3D potential problems can be generalized into the following form

$$I = \int_{\Gamma_e} \frac{f(\mathbf{x}, \mathbf{y})}{r^{2\alpha}} d\Gamma = \int_{\eta_j}^{\eta_{j+1}} \int_{\xi_i}^{\xi_{i+1}} \frac{f(\xi, \eta)}{r^{2\alpha}} d\xi d\eta \tag{24}$$

where Γ is, in general, an isogeometric element, $\alpha > 0$ is a real constant and $f(x, y)$ denotes a well-behaved function.

Note that in the integral representation (11), the kernel $u^*(\mathbf{x}, \mathbf{y})$ shows a near weak-singularity of order $(1/r)$ when $x \to y$, while the kernels $q^*(\mathbf{x}, \mathbf{y})$ have a near strong-singularity of order $\left(1/r^2\right)$. Here, these nearly singular integrals will be computed by the adaptive integration method.

4. Evaluation of 3D singular boundary integrals

As is well-known in BEM, when the source point $\mathbf{x}^P$ is located on the element under integration, the distance r may approach zero and therefore the singularity appears. Now, consider the 3D boundary integral $I^e(\mathbf{x}^P)$ on element e.

$$I^e(\mathbf{x}^P) = \int_{\Gamma_e} \frac{\bar{f}(\mathbf{x}^P, \mathbf{x})}{r^\beta(\mathbf{x}^P, \mathbf{x})} d\Gamma = \int_{\eta_j}^{\eta_{j+1}} \int_{\xi_i}^{\xi_{i+1}} \frac{\bar{f}(\mathbf{x}^P, \mathbf{x})}{r^\beta(\mathbf{x}^P, \mathbf{x})} d\xi d\eta \tag{25}$$

where β is a constant and $\bar{f}(\mathbf{x}^P, \mathbf{x})$ is bounded everywhere for the variable $\mathbf{x}$. Using the radial integration method (RIM) presented by Gao [57,58], the integral in Eq. (25) can be transformed into a contour ($L = \sum_{i=1}^{4} L_i$) integral along the four sides of the element, i.e.

$$I^e(\mathbf{x}^P) = \int_L \frac{1}{\rho(P, Q)} \frac{\partial \rho(P, Q)}{\partial \mathbf{n}'} F(\mathbf{x}^P, \mathbf{x}^Q) dL(Q) \tag{26}$$

where

$$F(\mathbf{x}^P, \mathbf{x}^Q) = \lim_{\rho_\alpha(\varepsilon) \to 0} \int_{\rho_\alpha(\varepsilon)}^{\rho(P,Q)} \frac{\bar{f}(\mathbf{x}^P, \mathbf{x})}{r^\beta(\mathbf{x}^P, \mathbf{x})} \left|J_{\xi\eta}\right| \rho d\rho \tag{27}$$

in which Q represents the field point which takes on a value from the boundary L as shown in Fig. 5, $\mathbf{n}'(n'_\xi, n'_\eta)$ is the outward normal to the boundary L of the integration boundary, ρ is the local distance defined as

$$\rho = \sqrt{(\xi - \xi_P)^2 + (\eta - \eta_P)^2}. \tag{28}$$

Following the method in papers [55,56], Eq. (27) can be given as

$$F(\mathbf{x}^P, \mathbf{x}^Q) = \sum_{k=0}^{K} B_k \lim_{\rho_\alpha(\varepsilon) \to 0} \int_{\rho_\alpha(\varepsilon)}^{\rho(Q,P)} \rho^{k-\beta+1} d\rho = \sum_{k=0}^{K} B_k E_k \tag{29}$$

where

$$E_k = \begin{cases} \dfrac{1}{k-\beta+2} \left[\dfrac{1}{\rho^{\beta-k-2}(Q, P)} - H_{\beta-k-2} \right], & 0 \le k \le \beta - 3 \\ \ln \rho(Q, P) - \ln H_0, & k = \beta - 2 \\ \dfrac{\rho^{k-\beta+2}(Q, P)}{k-\beta+2}, & k > \beta - 2 \end{cases} \tag{30}$$

and

$$\begin{aligned} &H_0 = 1/\bar{C}_0; \quad H_1 = \bar{C}_1; \quad H_2 = 2\bar{C}_2 - \bar{C}_1^2, \\ &H_3 = 3\bar{C}_3 - 3\bar{C}_1\bar{C}_2 + \bar{C}_1^3, \\ &H_4 = 4\bar{C}_4 + 4\bar{C}_1^2\bar{C}_2 - 4\bar{C}_1\bar{C}_3 - 2\bar{C}_2^2 - \bar{C}_1^4 \end{aligned} \tag{31}$$

in which $\bar{C}_i = C_i/C_0$. Coefficients B_k and C_i can be obtained by [55,56].

5. Numerical examples

To illustrate the accuracy and flexibility of 3D IGABEM, several 3D potential examples are now studied in which the proposed method is compared with the analytical solutions. In order to carry out accuracy and convergence analysis, an average relative error is given as

$$\text{Relative Error (RE)} = \left|I^k_{num} - I^k_{exact}\right| / \left|I^k_{exact}\right| \tag{32}$$

where I^k_{num} and I^k_{exact} denote the numerical and analytical solutions at the kth point, respectively.

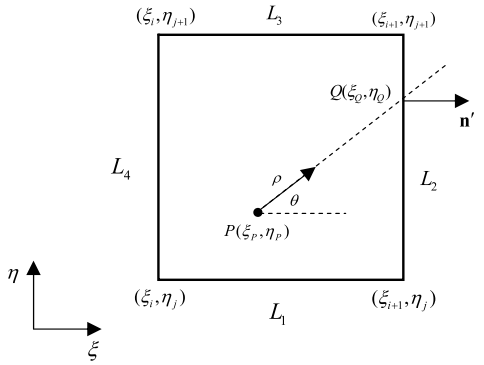

Fig. 5. Integration plane in intrinsic coordinate system.

Table 1
Polynomial orders and knot vectors for the isogeometric boundary element.

Direction	Order	Knot vector
ξ	$p = 2$	$\mathbf{U} = \{0, 0, 0, 1, 1, 1\}$
η	$q = 2$	$\mathbf{V} = \{0, 0, 0, 1, 1, 1\}$

Table 2
Control points for the element.

Control points	Coordinates	Weights
P_1	(1,0,0)	1
P_2	(1,1,0)	1
P_3	(1,2,0)	1
P_4	(1,0,1)	$\sqrt{2}/2$
P_5	(1,1,1)	$\sqrt{2}/2$
P_6	(1,2,1)	$\sqrt{2}/2$
P_7	(0,0,1)	1
P_8	(0,1,1)	1
P_9	(0,2,1)	1

5.1. Integral over 3D isogeometric cylindrical surface

To test our method and program, the following integral over an isogeometric cylindrical surface element is considered. The surface element is a 90° cylindrical panel with $r = 1$, $l = 2$ as shown in Fig. 6. The corresponding polynomial orders and knot vectors are given in Table 1 and control points are given in Table 2.

$$I(\boldsymbol{x}^p) = \int_S \frac{1}{4\pi r} dS. \tag{33}$$

Three source points (a, b and c) are computed with coordinates

$$x = r\cos\theta, \qquad y = \delta, \qquad z = r\sin\theta. \tag{34}$$

Points a and b are gradually close to the real boundary along the radii direction, whereas point c whose projective point to the boundary element is located outside the element (as shown in Fig. 1(b)) is moving along negative direction of y axis to the boundary of the element. Tables 3–5 list the computed results and the parameters for points a, b and c. Analytical results are easy to be obtained for this example and are also listed in the tables. From the three tables, it can be seen that the current results are in excellent agreement with the analytical results.

In addition, the results also tell us that, even if the source point is very close to the boundary of the element, good results can still be achieved. This is attributed to the use of subdivision technique to reduce the L_i/R ratio.

5.2. Integral over 3D degenerated isogeometric surface element

As is shown in Fig. 7 at the poles of a sphere, the quadrilateral element degenerates into triangular one. Therefore, we will test our method and program in this example. The corresponding polynomial orders and knot vectors of the isogeometric element are the same as Table 1 and control points are given in Table 6. The following integral over the degenerated

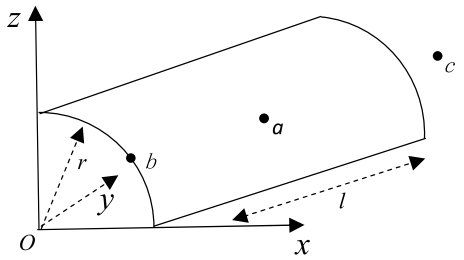

Fig. 6. Isogeometric cylindrical surface element.

Table 3
Computed results for the source point *a*.

Parameter			Adaptive solution	Exact solution
r	θ	δ		
0	$\pi/4$	1.0	0.22034340	0.22034340
0.2	$\pi/4$	1.0	0.25618639	0.25618639
0.4	$\pi/4$	1.0	0.30127012	0.30127012
0.6	$\pi/4$	1.0	0.35690961	0.35690961
0.8	$\pi/4$	1.0	0.42287711	0.42287722
0.9	$\pi/4$	1.0	0.45909425	0.45909405
0.99	$\pi/4$	1.0	0.49308607	0.49308609
0.999	$\pi/4$	1.0	0.49654503	0.49654503

Table 4
Computed results for the source point *b*.

Parameter			Adaptive solution	Exact solution
r	θ	δ		
0	$\pi/3$	0.0	0.18045443	0.18045443
0.2	$\pi/3$	0.0	0.20156155	0.20156155
0.4	$\pi/3$	0.0	0.22630790	0.22630790
0.6	$\pi/3$	0.0	0.25511481	0.25511480
0.8	$\pi/3$	0.0	0.28815709	0.28815717
0.9	$\pi/3$	0.0	0.30611233	0.30611232
0.99	$\pi/3$	0.0	0.32288670	0.32288671
0.999	$\pi/3$	0.0	0.32458861	0.32458861

Table 5
Computed results for the source point *c*.

Parameter			Adaptive solution	Exact solution
r	θ	δ		
1.0	$\pi/4$	3	0.13245723	0.13245704
1.0	$\pi/4$	2.8	0.14915621	0.14915423
1.0	$\pi/4$	2.6	0.17094257	0.17094272
1.0	$\pi/4$	2.4	0.20073741	0.20073774
1.0	$\pi/4$	2.2	0.24474818	0.24474870
1.0	$\pi/4$	2.1	0.27705734	0.27705794
1.0	$\pi/4$	2.01	0.32201384	0.32201384
1.0	$\pi/4$	2.001	0.32979372	0.32979372

isogeometric element is considered.

$$I(\boldsymbol{x}^p) = \frac{1}{4\pi}\int_S \frac{r_{,1}}{r^2} dS \left(r_{,1} = \frac{\partial r}{\partial x}\right). \tag{35}$$

In this example, source points e, f and g are considered. The coordinates of the points can be described as follows:

$$x = r\cos\theta\sin\phi; \qquad y = r\cos\theta\sin\phi; \qquad z = r\cos\phi \tag{36}$$

where $0 \le \theta \le 2\pi$ and $0 \le \phi \le \pi$. Fig. 8 plots the integral results of two source points $e\,(\theta, \phi) = (\pi/4, \pi/4)$ and $f\,(\theta, \phi) = (\pi/4, \pi/2)$ as the calculation point gets increasingly closer to the boundary along the radii direction. We observe that the current method can give very satisfactory results even when distance to the real boundary of the element is 0.001. In addition, Table 7 gives the results at point g with parameter $(r, \phi) = (1.0, \pi/4)$ and θ close to the boundary of the

Table 6
Control points for the integration element.

Control points	Coordinates	Weights
P_1	(1,0,0)	1
P_2	(1,1,0)	$\sqrt{2}/2$
P_3	(0,1,0)	1
P_4	(1,0,1)	$\sqrt{2}/2$
P_5	(1,1,1)	0.5
P_6	(0,1,1)	$\sqrt{2}/2$
P_7	(0,0,1)	1
P_8	(0,0,1)	$\sqrt{2}/2$
P_9	(0,0,1)	1

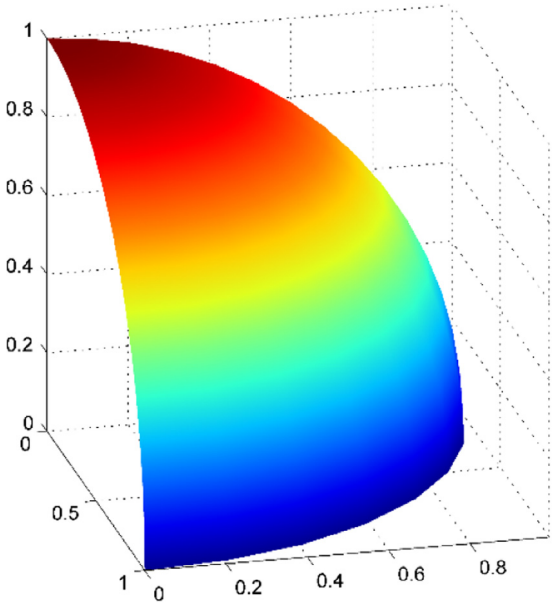

Fig. 7. The degenerated element.

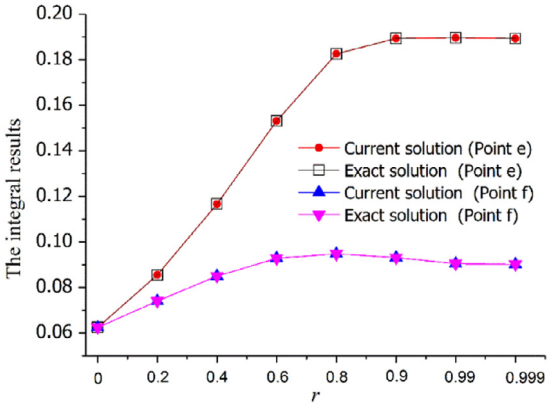

Fig. 8. Integral results of points e and f.

integration element. It is easy to see that the current results are very accurate and stable. This numerical example testifies that the present method is effective to solve the integral over 3D degenerated isogeometric surface element.

5.3. Potential problem over an ellipsoid model

A 3D ellipsoid surface is used for discussion, which is shown in Fig. 9. To describe this model the corresponding polynomial orders and knot vectors are given in Table 8 and control points are given in Fig. 11. Mesh of the isogeometric model is also

Table 7
Computed results for the source point g.

Parameter			Adaptive solution	Exact solution
r	θ	ϕ		
1.0	$24\pi/32$	$\pi/4$	0.11647795	0.11647795
1.0	$23\pi/32$	$\pi/4$	0.12947223	0.12947206
1.0	$22\pi/32$	$\pi/4$	0.14547478	0.14547517
1.0	$21\pi/32$	$\pi/4$	0.16567925	0.16567895
1.0	$20\pi/32$	$\pi/4$	0.19207403	0.19207504
1.0	$19\pi/32$	$\pi/4$	0.22839199	0.22839107
1.0	$18\pi/32$	$\pi/4$	0.28300264	0.28300340
1.0	$17\pi/32$	$\pi/4$	0.38274878	0.38274752

Table 8
Polynomial orders and knot vectors for the isogeometric boundary element.

Direction	Order	Knot vector
ξ	$p = 2$	$\mathbf{U} = \{0, 0, 0, 1, 1, 2, 2, 3, 3, 4, 4, 4\}$
η	$q = 2$	$\mathbf{V} = \{0, 0, 0, 1, 1, 1\}$

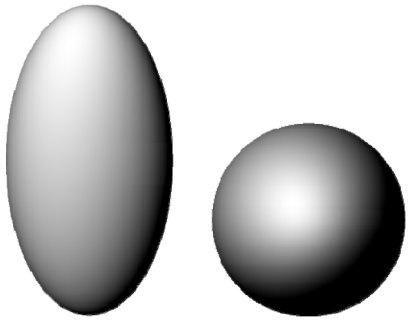

(a) Front view. (b) Vertical view.

Fig. 9. The isogeometric model of the ellipsoid.

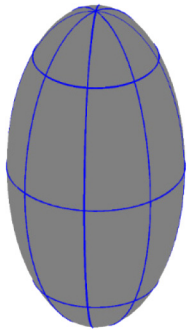

Fig. 10. The mesh of the model.

shown in Fig. 10. As shown in Fig. 10, the quadrilateral elements degenerate into triangular elements at the two poles of the model. The potential on the boundary is given as $u = 5x - 3y + z + 1$.

Fig. 12(a) shows the numerical results of potential when the computed points are gradually close to the boundary along the line $x = R\cos(\pi/4)$, $y = R\sin(\pi/4)$, $z = 0$ on the x–y plane and the exact solutions are given as comparison. It can be observed that the results obtained by both the conventional IGABEM and present method are satisfactory when $d \geq 0.1$. As the interior point further approaches the outer boundary, the results obtained by the conventional IGABEM are totally invalid. On the other hand, the present method can obtain accurate results even when the distance between the interior point and the outer boundary is as small as 0.001. Fig. 12(b) gives the results when the source points are close to the poles along positive direction of Z axis. Fig. 12(b) also tells us that when the distance is bigger than 0.07 the results obtained by the two methods are consistent with the exact solution. However, with the decrease of distance the conventional method becomes unstable and even invalid. On the contrary, the results obtained by the current method are still effective.

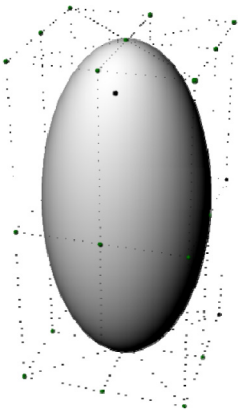

Fig. 11. The control points of the model.

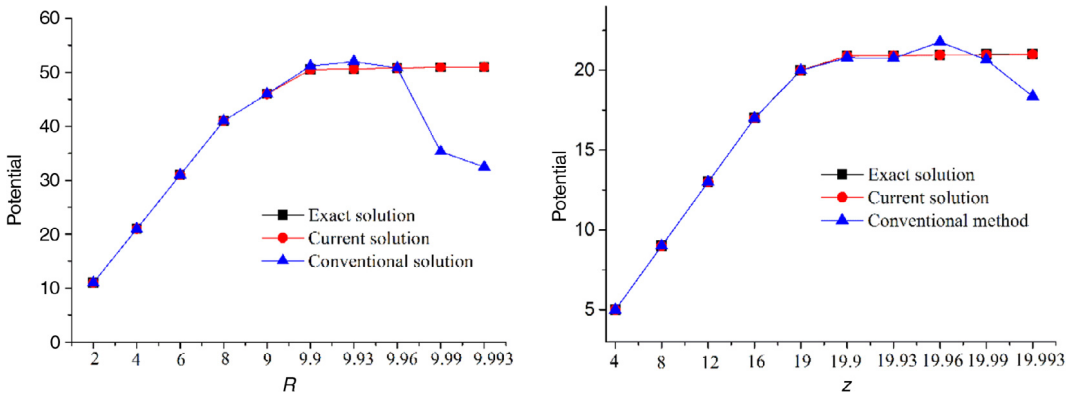

(a) Results close to the boundary on the x–y plane.

(b) Results close to the poles.

Fig. 12. The potentials at the points being gradually close to the boundary.

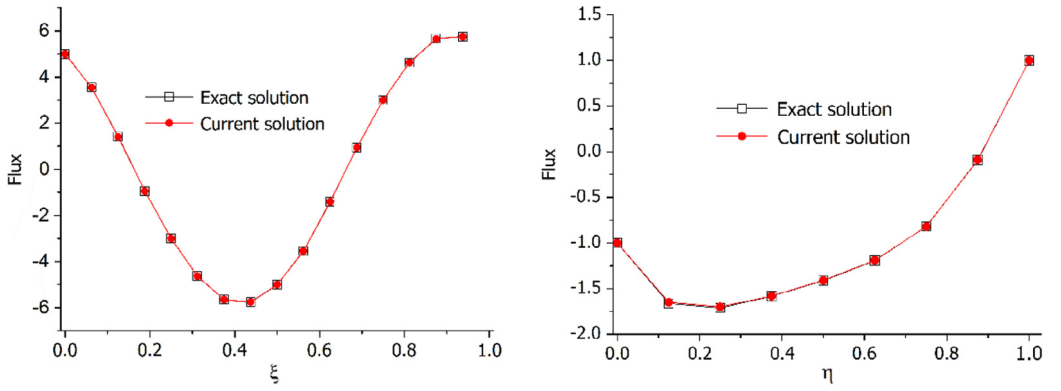

(a) Results along the latitude with (ξ, $\eta = 0.5$).

(b) Results along the longitude with ($\xi = 0.625$, η).

Fig. 13. The computed results of normal flux q on the surface.

In addition, the results of normal flux q on the surface along the latitude with parameter coordinate (ξ, $\eta = 0.5$) are given in Fig. 13(a). Fig. 13(b) shows the numerical results of flux q on surface points along the longitude with parameter coordinate ($\xi = 0.625$, η), from which it can be seen that the current results are in good agreement with the exact results. This numerical example testifies again that the present method is effective to solve the potential problems.

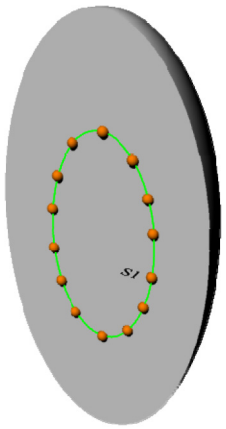

Fig. 14. The computed internal points along curve S1.

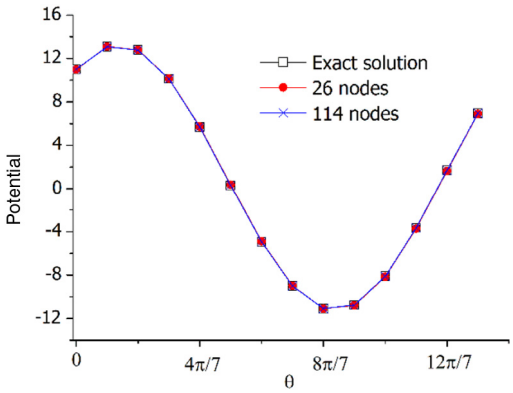

Fig. 15. The numerical results of potential on curve S1.

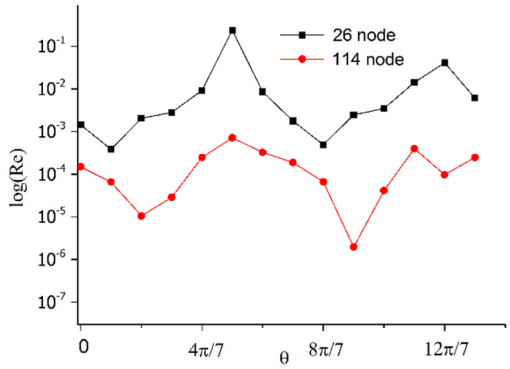

Fig. 16. The relative errors of the two sets of nodes.

In order to study the convergence rate, two sets of nodes, i.e. (a) 26 and (b) 114, have been used for discretization of the body surface. The potential u inside the model along the following curve (Fig. 14) is considered.

$$\text{S1} : x = a\cos\theta\sin\phi, \qquad y = b\sin\theta\sin\phi, \qquad z = c\cos\phi \tag{37}$$

where $a = b = 5, c = 10$.

Fig. 15 gives the numerical results of potential on curve S1 and the exact solutions are also given as comparison. The relative errors of the two sets of nodes are shown in Fig. 16. From Figs. 15 and 16, we can observe that the results converge to the exact solution on the body surfaces very well and the relative error of the computed points is small and convergent with the increase of nodes.

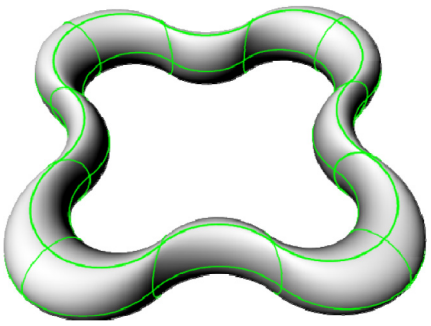

Fig. 17. The isogeometric model of 3D complex surface.

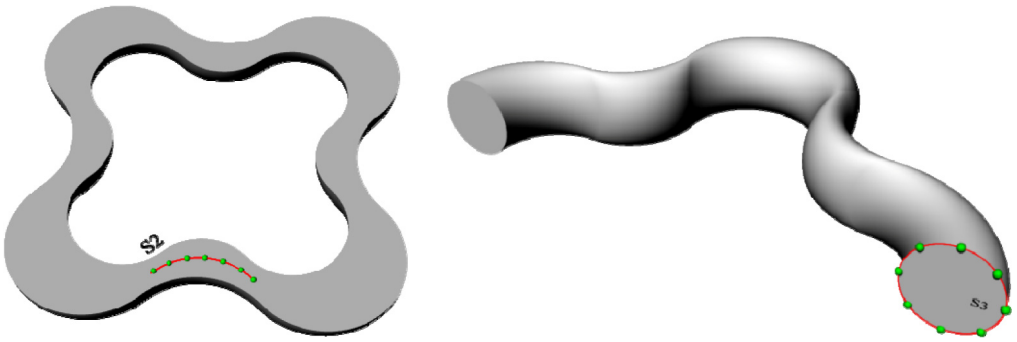

(a) Points along curve S2. (b) Points along curve S3.

Fig. 18. The computed points model.

5.4. Potential problem over a complex isogeometric model

Finally, to illustrate the ability of presented method to handle arbitrary geometries which can be taken directly from CAD, a problem with complex surface as shown in Fig. 17 is analyzed. The physical quantities on the boundary surface are given as follows.

$$u = 5x + 6y + 7z + 7/5. \tag{38}$$

For this example, two sets of nodes, i.e. (a) 192 nodes and (b) 768 nodes, are used for the discretization of the body surfaces. Table 9 shows the numerical results of potential when the computed points are moving along the following curve (S2, as is shown in Fig. 18(a)) and the exact solutions are given as comparison.

$$\text{S2} : x = R\cos\theta, \qquad y = R\sin\theta, \qquad z = 0 \tag{39}$$

where $R = 15$. From Table 9, we can clearly see that the current solutions are in good agreement with the exact results. For interior points, the results obtained by 192 nodes are already very accurate. With the increase of the computed nodes, the relative errors of the numerical results decrease significantly, which means the proposed method is convergent.

In addition, 8 boundary points (see Fig. 18(b)) on the surface of the model are taken into account. Fig. 19 gives the relative errors (Re) of numerical results of q along the curve S3. It is easy to see that the numerical results are convergent to the exact solutions with the increase of nodes on the body surfaces. It can be seen that the proposed method is accurate and stable for this potential problem over the complex isogeometric model.

6. Conclusions

In this paper, 3D IGABEM using adaptive integral method for potential problems has been presented. In the adaptive integral method, a specified maximum of Gauss order is given beforehand. During the process of integration, if the required Gauss integration order exceeds the maximum, the integration elements will be divided into sub-elements. This method adaptively increases Gauss orders as the source point in integral equation approaches the boundary of isogeometric element and subdivides the element into sub-elements to avoid using excessively high Gauss order according to Davies and Bu's criterion [60]. Thus, this method delivers high accuracy at optimal computational cost for 3D boundary integrals on isogeometric element method. In addition, the adaptive integration method is based on element sub-division technique, namely, reducing the distance ratio (L_i/R). Thus, the nearly singular integrals appearing in the IGABEM can be computed effectively by the presented method.

Table 9
The numerical results of potential when the computed points are moving along the curve S2.

Points coordinates			Exact solution	192 nodes		768 nodes	
x	y	z		Numerical results	Error	Numerical results	Error
−0.100E+02	−0.200E+02	0.000E+00	−0.1686000E+03	−0.1686188E+03	0.1112660E−03	−0.1685995E+03	0.2801511E−05
−0.103E+02	−0.174E+02	0.000E+00	−0.1547746E+03	−0.1547661E+03	0.5492941E−04	−0.1547750E+03	0.2645754E−05
−0.113E+02	−0.150E+02	0.000E+00	−0.1452987E+03	−0.1452882E+03	0.7240593E−04	−0.1452994E+03	0.4516060E−05
−0.129E+02	−0.129E+02	0.000E+00	−0.1408183E+03	−0.1408074E+03	0.7704446E−04	−0.1408185E+03	0.1486882E−05
−0.150E+02	−0.113E+02	0.000E+00	−0.1416385E+03	−0.1416230E+03	0.1091073E−03	−0.1416390E+03	0.3352263E−05
−0.174E+02	−0.103E+02	0.000E+00	−0.1477035E+03	−0.1476925E+03	0.7432114E−04	−0.1477038E+03	0.1852870E−05
−0.200E+02	−0.100E+02	0.000E+00	−0.1586000E+03	−0.1586244E+03	0.1536316E−03	−0.1585997E+03	0.2179586E−05

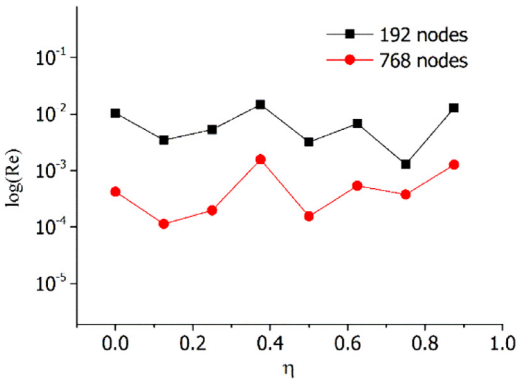

Fig. 19. The relative errors (Re) of numerical results of q along the curve S3.

To accurately evaluate the singular integrals appearing in our method, the power series expansion method is employed, in which the non-singular part of a singular integrand as well as the global distance r is expressed as power series in the local distance ρ of the intrinsic coordinate system. Contrast to the original power series expansion method, one of the features of the present method is that the integration surface is on the real surface of the model, rather than the interpolation surface, i.e. no geometrical errors. Thus, the value of integral is more accurate than the traditional boundary element method.

The proposed method offers great advantages in the numerical evaluation of nearly singular integrals that appear in the thin-body/coating structures with uneven thickness. Some work along this line is already underway and will be reported in a future paper.

Acknowledgment

The research is supported by the National Natural Science Foundation of China (11272054, 11672038).

References

[1] T.J. Hughes, J.A. Cottrell, Y. Bazilevs, Isogeometric analysis: CAD, finite elements, NURBS, exact geometry and mesh refinement, Comput. Methods Appl. Mech. Engrg. 194 (2005) 4135–4195.
[2] Y. Bazilevs, V.M. Calo, Y. Zhang, T.J.R. Hughes, Isogeometric fluid–structure interaction analysis with applications to arterial blood flow, Comput. Mech. 38 (2006) 310–322.
[3] Y. Bazilevs, T.J.R. Hughes, Weak imposition of Dirichlet boundary conditions in fluid mechanics, Comput. & Fluids 36 (2007) 12–26.
[4] Y. Bazilevs, V.M. Calo, T.J.R. Hughes, Y. Zhang, Isogeometric fluid–structure interaction: theory, algorithms, and computations, Comput. Mech. 43 (2008) 3–37.
[5] J.A. Cottrell, A. Reali, Y. Bazilevs, T.J.R. Hughes, Isogeometric analysis of structural vibrations, Comput. Methods Appl. Mech. Engrg. 195 (2006) 5257–5296.
[6] J.A. Cottrell, T.J.R. Hughes, A. Reali, Studies of refinement and continuity in isogeometric structural analysis, Comput. Methods Appl. Mech. Engrg. 196 (2007) 4160–4183.
[7] S.H. Ha, K.K. Choi, S. Cho, Numerical method for shape optimization using T-spline based isogeometric method, Struct. Multidiscip. Optim. 42 (2010) 417–428.
[8] P. Fischer, M. Klassen, J. Mergheim, P. Steinmann, R. Müller, Isogeometric analysis of 2D gradient elasticity, Comput. Mech. 47 (2011) 325–334.
[9] L. De Lorenzis, J. Evans, T. Hughes, A. Reali, Isogeometric collocation: Neumann boundary conditions and contact, Comput. Methods Appl. Mech. Engrg. 284 (2015) 21–54.
[10] P. Kang, S.K. Youn, Isogeometric analysis of topologically complex shell structures, Finite Elem. Anal. Des. 99 (2015) 68–81.
[11] R. Bouclier, T. Elguedj, A. Combescure, An isogeometric locking-free NURBS-based solid-shell element for geometrically nonlinear analysis, Internat. J. Numer. Methods Engrg. 101 (10) (2015) 774–808.
[12] C. Politis, A.I. Ginnis, P.D. Kaklis, K. Belibassakis, C. Feurer, An isogeometric BEM for exterior potential-flow problems in the plane, in: 2009 SIAM/ACM. Proceedings of the joint conference on geometric and physical modeling, SPM'09 2009: pp. 349–54.
[13] K. Li, X. Qian, Isogeometric analysis and shape optimization via boundary integral, Comput. Aided Des. 43 (2011) 1427–1437.
[14] R.N. Simpson, S.P.A. Bordas, J. Trevelyan, T. Rabczuk, A two-dimensional isogeometric boundary element method for elastostatic analysis, Comput. Methods Appl. Mech. Engrg. 209–212 (2012) 87–100.

[15] R.N. Simpson, S.P.A. Bordas, H. Lian, J. Trevelyan, An isogeometric boundary element method for elastostatic analysis: 2D implementation aspects, Comput. Struct. 118 (2013) 2–12.
[16] Y. Bai, C.Y. Dong, Z.Y. Liu, Effective elastic properties and stress states of doubly periodic array of inclusions with complex shapes by isogeometric boundary element method, Compos. Struct. 128 (2015) 54–69.
[17] J.L. Gu, J.M. Zhang, L.F. Chen, Z.H. Cai, An isogeometric BEM using PB-spline for 3-D linear elasticity problem, Eng. Anal. Bound. Elem. 56 (2015) 154–161.
[18] A. Aimi, M. Diligenti, M.L. Sampoli, A. Sestini, Isogemetric analysis and symmetric Galerkin BEM: A 2D numerical study, Appl. Math. Comput. 272 (2016) 173–186.
[19] T. Takahashi, T. Matsumoto, An application of fast multipole method to isogeometric boundary element method for Laplace equation in two dimensions, Eng. Anal. Bound. Elem. 36 (2012) 1766–1775.
[20] R.N. Simpson, Z. Liu, Acceleration of isogeometric boundary element analysis through a black-box fast multipole method, Eng. Anal. Bound. Elem. 66 (2016) 168–182.
[21] M.J. Peake, J. Trevelyan, G. Coates, Extended isogeometric boundary element method (XIBEM) for two-dimensional Helmholtz problems, Comput. Methods Appl. Mech. Engrg. 259 (2013) 93–102.
[22] K.A. Belibassakis, Th.P. Gerostathis, K.V. Kostas, C.G. Politis, P.D. Kaklis, A.I. Ginnis, C. Feurer, A BEM-isogeometric method for the ship wave-resistance problem, Ocean Eng. 60 (2013) 53–67.
[23] A.I. Ginnisa, K.V. Kostasb, C.G. Politisb, P.D. Kaklisa, K.A. Belibassakisa, Th.P. Gerostathisb, M.A. Scottd, T.J.R. Hughes, Isogeometric boundary-element analysis for the wave-resistance problem using T-splines, Comput. Methods Appl. Mech. Engrg. 279 (2014) 425–439.
[24] R.N. Simpson, M.A. Scott, M. Taus, D.C. Thomas, H. Lian, Acoustic isogeometric boundary element analysis, Comput. Methods Appl. Mech. Engrg. 269 (2014) 265–290.
[25] M.J. Peake, J. Trevelyan, G. Coates, Extended isogeometric boundary element method (XIBEM) for three-dimensional medium-wave acoustic scattering problems, Comput. Methods Appl. Mech. Engrg. 284 (2015) 762–780.
[26] K.V. Kostas, A.I. Ginnis, C.G. Politis, P.D. Kaklis, Ship-hull shape optimization with a T-spline based BEM–isogeometric solver, Comput. Methods Appl. Mech. Engrg. 284 (2015) 611–622.
[27] E. Gillebaart, R. De Breuker, Low-fidelity 2D isogeometric aeroelastic analysis and optimization method with application to a morphing airfoil, Comput. Methods Appl. Mech. Engrg. 305 (2016) 512–536.
[28] Minho Yoon, Seonho Cho, Isogeometric shape design sensitivity analysis of elasticity problems using boundary integral equations, Eng. Anal. Bound. Elem. 66 (2016) 119–128.
[29] Y.J. Wang, D.J. Benson, Multi-patch nonsingular isogeometric boundary element analysis in 3D, Comput. Methods Appl. Mech. Engrg. 293 (2015) 71–91.
[30] M. Feischl, G. Gantner, D. Praetorius, Reliable and efficient a posteriori error estimation for adaptive IGA boundary element methods for weakly-singular integral equations, Comput. Methods Appl. Mech. Engrg. 290 (2015) 362–386.
[31] B.H. Nguyen, H.D. Tran, C. Anitescu, X. Zhuang, T. Rabczuk, An isogeometric symmetric Galerkin boundary element method for two-dimensional crack problems, Comput. Methods Appl. Mech. Engrg. 306 (2016) 252–275.
[32] M. Feischl, G. Gantner, A. Haberl, D. Praetorius, Adaptive 2D IGA boundary element methods, Eng. Anal. Bound. Elem. 62 (2016) 141–153.
[33] X.W. Gao, T.G. Davies, Adaptive integration in elastoplastic boundary element analysis, J. Chin. Inst. Eng. 23 (3) (2000) 349–356.
[34] X.W. Gao, T.G. Davies, Boundary Element Programming in Mechanics, Camberidge University Press, 2002.
[35] Y.M. Zhang, Y.P. Gong, X.W. Gao, Calculation of 2D nearly singular integrals over high-order geometry elements using the sinh transformation, Eng. Anal. Bound. Elem. 60 (2015) 144–153.
[36] G.Z. Xie, J.M. Zhang, Y.Q. Dong, C. Huang, G.Y. Li, An improved exponential transformation for nearly singular boundary element integrals in elasticity problems, Internat. J. Solids Structures 51 (2014) 1322–1329.
[37] Y. Gu, H.W. Gao, W. Chen, C.Z. Zhang, A general algorithm for evaluating nearly singular integrals in anisotropic three-dimensional boundary element analysis, Comput. Methods Appl. Mech. Engrg. 308 (2016) 483–498.
[38] Y. Gu, Q. Hua, W. Chen, et al., Numerical evaluation of nearly hyper-singular integrals in the boundary element analysis, Comput. Struct. 167 (2016) 15–23.
[39] X.Y. Qin, J.M. Zhang, G.Z. Xie, F.L. Zhou, G.Y. Li, A general algorithm for the numerical evaluation of nearly singular integrals on 3D boundary element, J. Comput. Appl. Math. 235 (2011) 4174–4186.
[40] W. John, T.K. Tsay, Analytical evaluation and application of the singularities in boundary element method, Eng. Anal. Bound. Elem. 29 (2005) 241–256.
[41] G.S. Padhi, R.A. Shenoi, S.S.J. Moy, et al., Analytical Integration of kernel shape function product integral in the boundary element method, Comput. Struct. 79 (2001) 1325–1333.
[42] M.A. Lifeng, A.M. Korsunsky, A note on the Gauss-Jacobi quadrature formulae for singular integral equations of the second kind, Int. J. Fract. 126 (2004) 339–405.
[43] O. Huber, A. Lang, G. Kuhn, Evaluation of the stress tensor in 3D elastostatics by direct solving of hyper singular integrals, Comput. Mech. 12 (1993) 39–50.
[44] G. Karami, D. Derakhshan, An efficient method to evaluate hyper singular and super singular integrals in boundary integral equations analysis, Eng. Anal. Bound. Elem. 23 (1999) 317–326.
[45] J.C.F. Telles, A self-adaptive coordinate transformation for efficient numerical evaluation of general boundary element integrals, Internat. J. Numer. Methods Engrg. 24 (1987) 959–973.
[46] M. Cerrolaza, E. Alarcón, A bi-cubic transformation for the numerical evaluation of the Cauchy principal value integrals in boundary methods, Internat. J. Numer. Methods Engrg. 28 (1989) 987–999.
[47] Z.R. Niu, H.L. Zhou, A novel boundary integral equation method for linear elasticity-natural boundary integral equation, Acta Mech. Solida Sin. 14 (2001) 1–10.
[48] H.R. Kutt, The numerical evaluation of principal value integrals by finite-part integration, Numer. Math. 24 (1975) 205–210.
[49] H.R. Kutt, Quadrature formulae for finite-part integrals, Technical Report CSIR Special Report WISK 178, National Research Institute for Mathematical Sciences CSIR, South Africa, 1975.
[50] J. Dominguez, M.P. Ariza, R. Gallego, Flux and traction boundary elements without hyper singular or strongly singular integrals, Internat. J. Numer. Methods Engrg. 48 (2000) 111–135.
[51] A.B. Jorge, G.O. Ribeiro, T.A. Cruse, et al., Self-regular boundary integral equation formulations for Laplace's equation in 2-D, Internat. J. Numer. Methods Engrg. 51 (2001) 1–29.
[52] M. Guiggiani, P. Casalini, Direct computation of Cauchy principal value integrals in advanced boundary elements, Internat. J. Numer. Methods Engrg. 24 (1987) 1711–1720.
[53] M. Guiggiani, G. Krishnasamy, T.J. Rudolphi, et al., General algorithm for the numerical solution of hyper-singular boundary integral equations, J. Appl. Mech. 59 (1992) 604–614.
[54] X.W. Gao, K. Yang, J. Wang, An adaptive element subdivision technique for evaluation of various 2D singular boundary integrals, Eng. Anal. Bound. Elem. 32 (2008) 692–696.
[55] X.W. Gao, Numerical evaluation of two-dimensional singular boundary integrals-Theory and Fortran code, J. Comput. Appl. Math. 188 (2006) 44–64.
[56] X.W. Gao, An effective method for numerical evaluation of general 2D and 3D high order singular boundary integrals, Comput. Methods Appl. Mech. Engrg. 199 (2010) 2856–2864.
[57] X.W. Gao, The radial integration method for evaluation of domain integrals with boundary-only discretization, Eng. Anal. Bound. Elem. 26 (2002) 905–916.

[58] X.W. Gao, A boundary element method without internal cells for two-dimensional and three-dimensional elastoplastic problems, J. Appl. Mech. 69 (2002) 154–160.
[59] G.G.W. Mustoe, Advanced integration schemes over boundary elements and volume cells for two- and three-dimensional non-linear analysis, in: P.K. Banerjee, S. Mukherjee (Eds.), Developments in Boundary Element Methods - 3, Elsevier, London, 1984, pp. 213–270.
[60] T.G. Davies, S. Bu, Effective evaluation of non-singular integrals in 3D BEM, Adv. Eng. Softw. 23 (1995) 121–128.